200500324A

厚生労働科学研究研究費補助金

長寿科学総合研究事業

老年期痴呆症における痴呆病態の基盤の解明に関する研究

平成１７年度　総括研究報告書

主任研究者　　木下　彩栄

平成１８年（２００６年）４月５日

目次

厚生労働科学研究費補助金（長寿科学総合研究事業）
（総括）研究報告書

老年期痴呆症の痴呆病態の基盤の解明に関する研究

(主任)研究者　木下彩栄　京都大学教授

研究要旨　アルツハイマー病ではシナプスの変性が初期から観察されるが、現在までにその原因は解明されていない。われわれは、現在までの細胞レベルの実験結果で、実際に家族性アルツハイマー病の原因遺伝子であるプレセニリン(PS1)がシナプス蛋白の転写を調整していること、変異 PS1 ではこの働きが失われていることを解明してきた。さらに、この点に着目したモデルマウスを作成し、シナプス変性の病態の解明に役立てる。

分担研究者　植村健吾・京都大学・助手

A.　　研究目的

アルツハイマー病で初期から見られるシナプス変性の原因を解明するために、原因遺伝子であるプレセニリンの機能に着目してモデルマウスを作成する。

B.　　研究方法

遺伝子工学を用いて、シナプス蛋白である N-cadherin に PS1 で切断を受けない変異を導入し、これをベクターに組み込み、ES 細胞に導入する。さらにこれをスクリーニングして、陽性のクローンからキメラマウスを作成し、ノックインマウスの F1 を作成する。

C．研究結果

B によって行われた遺伝子改変マウスは現在陽性のクローンをいくつか得ることができ、現在キメラマウスを作成中である。

D．　考察

これにより、分担研究者が in vitro で見いだしたプレセニリンのシナプス蛋白の制御が in vivo でも同様なメカニズムが働いているかを検証する意義は大きい。さらに、このプレセニリンの機能障害がアルツハイマー病にどのように関わっているかを調べることにより、病態の解明を目指すことが可能になると期待される。

E．結論

上記のように、１年目としては十分な結果をだすことができた。モデルマウスが完成すれば、病理学的、行動学的、生化学的、生理学的に変化を解析し、PS1 がシナプス蛋白の制御に果たす生理的な役割や、その病的意義を確立することができると期待される。

G．研究発表

１．論文発表

Uemura, K., Kuzuya, A., Okawa, K., Ihara, M., Kinoshita, A. *, Shimohama, S. *:
PS1/N-cadherin interaction is required for the ipsilon-cleavage of human N-cadherin. Neurosci Lett (submitted) (2006) (*shared last author)

Uemura, K., Kihara, T., Kuzuya, A., Okawa, K., Nishimoto, T., Bito, H., Sugimoto, H., Shimohama, S.*, r*: Activity-dependent beta-catenin transcription via PS1/ipsilon-cleavage of N-cadherin by gamma-secretase complex. **Neurosci Lett** (submitted) (2006) (*shared last author)

Ihara, M., Kinoshita, A., Yamada, S., Tanaka, H., Tanigaki, A., Kitano, A., Goto, M., Okubo, K., Nishiyama, H., Ogawa, O., Takahashi, C., Itohara, S., Nishimune, Y., Noda, M., Kinoshita, M.: Cortical organization by the septin cytoskeleton is essential for structural and mechanical integrity of mammalian spermatozoa. Dev Cell. 8: 343-52, 2005

von Arnim, C. A.*, Kinoshita, A.*, Peltan, I. D., Tangredi , M. M., Herl, L., Lee, B. M., Spoelgen, R., Hshieh, T. T., Ranganathan, S., Battey, F. D., Liu, C. X., Bacskai , B. J., Sever, S., Irizarry, M. C., Strickland, D. K., Hyman, B. T.: The low density lipoprotein receptor-related protein (LRP) is a novel β-secretase (BACE1) substrate. J Biol Chem. 280:17777-85, 2005 (*shared first author)

2. 学会発表

木下彩栄 アルツハイマー病と APP トラフィッキング 第83回日本生理学大会 シンポジウム

植村健吾 他、プレセニリン1によるN-カドヘリン切断に関する研究 第46回日本神経学会(鹿児島)

Uemura K et al., ACTIVITY-DEPENDENT b-CATENIN TRANSCRIPTION VIA PS1/e-CLEAVAGE OF N-CADHERIN BY g-SECRETASE COMPLEX 第35回米国神経科学会 (米国、ワシントン)

H. 知的財産権の出願・登録状況

なし

厚生労働科学研究費補助金（長寿科学総合研究事業）
（分担）研究報告書

老年期痴呆症の痴呆病態の基盤の解明に関する研究

(分担)研究者　植村健吾　京都大学助手

研究要旨　アルツハイマー病ではシナプスの変性が初期から観察されるが、現在までにその原因は解明されていない。われわれは、家族性アルツハイマー病の原因遺伝子であるプレセニリン(PS1)がシナプス蛋白である N-cadherin の切断を制御し、Wnt シグナルを調整していること、変異 PS1 ではこの働きが失われていることを見出した。さらに、この制御は、老人班に蓄積しているアミロイドにより抑制されていることを見出した。これらの発見をアルツハイマー病の病態の解明に役立てる。

A.　研究目的

アルツハイマー病で初期から見られるシナプス変性の原因を解明するために、原因遺伝子であるプレセニリンのシナプス制御機構を解明する

B.　研究方法

遺伝子工学を用いて、シナプス蛋白である N-cadherin に PS1 で切断を受けない変異を導入し、これをベクターに組み込み、ES 細胞に導入する。さらにこれをスクリーニングして、陽性のクローンからキメラマウスを作成し、ノックインマウスの F1 を作成する。

C．研究結果

B によって行われた遺伝子改変マウスは現在陽性のクローンをいくつか得ることができ、現在キメラマウスを作成中である。

D.　考察

これにより、分担研究者が in vitro で見いだしたプレセニリンのシナプス蛋白の制御が in vivo でも同様なメカニズムが働いているかを検証する意義は大きい。さらに、このプレセニリンの機能障害がアルツハイマー病にどのように関わっているかを調べることにより、病態の解明を目指すことが可能になると期待される。

E．結論

上記のように、１年目としては十分な結果をだすことができた。モデルマウスが完成すれば、病理学的、行動学的、生化学的、生理学的に変化を解析し、PS1 がシナプス蛋白の制御に果たす生理的な役割や、その病的意義を確立することができると期待される。

G．研究発表

１．論文発表

Uemura, K., Kuzuya, A., Okawa, K., Ihara, M., Kinoshita, A. *, Shimohama, S. *:
PS1/N-cadherin interaction is required for the ipsilon-cleavage of human N-cadherin. Neurosci

	Lett (submitted) (2006) (*shared last author)

研究成果の刊行に関する一覧表レイアウト

書籍

なし

雑誌

発表者氏名	論文タイトル名	発表雑誌	巻号	ページ	出版年
Ihara, M., Kinoshita, A., Yamada, S., Tanaka, H., Tanigaki, A., Kitano, A., Goto, M., Okubo, K., Nishiyama, H., Ogawa, O., Takahashi, C., Itohara, S., Nishimune, Y., Noda, M., Kinoshita, M.	Cortical organization by the septin cytoskeleton is essential for structural and mechanical integrity of mammalian spermatozoa.	Developmental Cell	8	343-352	2005
von Arnim, C. A.*, Kinoshita, A.*, Peltan, I. D., Tangredi , M. M., Herl, L., Lee, B. M., Spoelgen, R., Hshieh, T. T., Ranganathan, S., Battey, F. D., Liu, C. X., Bacskai , B. J., Sever, S., Irizarry, M. C.,	The low density lipoprotein receptor-related protein (LRP) is a novel β-secretase (BACE1) substrate.	Journal of Biological Chemistry	280	17777-85	2005

Strickland, D. K., Hyman, B. T					

Developmental Cell, Vol. 8, 343–352, March, 2005, Copyright ©2005 by Elsevier Inc. DOI 10.1016/j.devcel.2004.12.005

Cortical Organization by the Septin Cytoskeleton Is Essential for Structural and Mechanical Integrity of Mammalian Spermatozoa

Masafumi Ihara,[1] Ayae Kinoshita,[2] Shuichi Yamada,[3] Hiromitsu Tanaka,[4] Ai Tanigaki,[5] Ayumi Kitano,[1] Motohito Goto,[3] Kazutoshi Okubo,[6] Hiroyuki Nishiyama,[6] Osamu Ogawa,[6] Chiaki Takahashi,[7] Shigeyoshi Itohara,[8] Yoshitake Nishimune,[4] Makoto Noda,[7] and Makoto Kinoshita[1,5,*]

[1] Biochemistry and Cell Biology Unit
[2] Alzheimer Research Unit
HMRO
Kyoto University Graduate School of Medicine
Kyoto
[3] Institute for Virus Research
Kyoto University
Kyoto
[4] Department of Science for Laboratory Animal Experimentation
Research Institute for Microbial Diseases
Osaka University
Suita
[5] PRESTO
Japan Science and Technology Agency
Kawaguchi
Japan
[6] Department of Urology
[7] Department of Molecular Oncology
Kyoto University Graduate School of Medicine
Kyoto
[8] Laboratory for Behavioral Genetics
RIKEN Brain Science Institute
Wako
Japan

Summary

Septins are polymerizing GTP binding proteins required for cortical organization during cytokinesis and other cellular processes. A mammalian septin gene *Sept4* is expressed mainly in postmitotic neural cells and postmeiotic male germ cells. In mouse and human spermatozoa, SEPT4 and other septins are found in the annulus, a cortical ring which separates the middle and principal pieces. *Sept4*$^{-/-}$ male mice are sterile due to defective morphology and motility of the sperm flagellum. In *Sept4* null spermatozoa, the annulus is replaced by a fragile segment lacking cortical material, beneath which kinesin-mediated intraflagellar transport stalls. The sterility is rescued by injection of sperm into oocytes, demonstrating that each *Sept4* null spermatozoon carries an intact haploid genome. The annulus/septin ring is also disorganized in spermatozoa from a subset of human patients with asthenospermia syndrome. Thus, cortical organization based on circular assembly of the septin cytoskeleton is essential for the structural and mechanical integrity of mammalian spermatozoa.

*Correspondence: mkinoshita@hmro.med.kyoto-u.ac.jp

Introduction

The septins are a family of polymerizing GTP binding proteins originally discovered in budding yeast as a group of cell cycle mutants which cause defects in cytokinesis (Field and Kellogg, 1999). Loss or mutation of any one of the five septins commonly results in multinuclear and multilocular morphology. These mutants lack electron-dense circular striations which are normally organized beneath the plasma membrane between a mother cell and the bud (Byers and Goetsch, 1976; Frazier et al., 1998). These circular striations represent the "septin ring," a subcellular structure which can be visualized by immunofluorescence or by the expression of septins fused to biofluorescent proteins. To date, the septin ring has been known to play multiple roles in cytokinesis: it serves as a scaffold for various mitosis-associated molecules (Gladfelter et al., 2001) and for positioning the mitotic spindle (Kusch et al., 2002), and as a diffusion barrier for partitioning membrane domains between a mother cell and the bud (Barral et al., 2000; Takizawa et al., 2000). Although such a structure and its related functions have not been demonstrated in higher organisms, requirement of the septin cytoskeleton for cytokinesis seems conserved up to mammals (Neufeld and Rubin 1994; Kinoshita et al., 1997; Nguyen et al., 2000).

Despite the progress of septin biology in yeast, many questions unique to the metazoan septin system remain unsolved: (1) Septins are abundantly expressed in nondividing cells, but little is known about their roles in postmitotic events (Beites et al., 1999; Adam et al., 2000; Dent et al., 2002; Finger et al., 2003). (2) Although mammalian septin filaments can self-organize circular bundles both in vitro and in interphase tissue culture cells following actin perturbation (Kinoshita et al., 2002), the physiological relevance of this unique property has not been established because a similar structure has not been found in vivo. (3) Although most septins are believed to function as cytoskeletal proteins, a few septin gene products are implicated in mitochondrial functions, apoptosis, and/or tumorigenesis. For instance, the human and mouse *Sept4* genes respectively generate polypeptides of 32 and 46 kDa in addition to the larger 48–54 kDa cytoskeletal isoforms. The 32 and 46 kDa isoforms are targeted to mitochondria in tissue culture cells, and the 32 kDa isoform induces cell death when overexpressed (Larisch et al., 2000; Takahashi et al., 2003). Messenger RNA for the 32 kDa "proapoptotic" isoform is downregulated during malignant progression of human lymphoma (Elhasid et al., 2004). Thus, *Sept4* is thought to be a potential tumor-suppressor gene in humans. However, it has also been claimed that *Sept4* is an oncogene whose upreg-

ulation is responsible for human colon cancer (Tanaka et al., 2002). As yet, these contradictory hypotheses have not been critically tested for relevance in vivo.

To address the puzzling situation regarding mammalian septins, especially SEPT4, we disrupted the *Sept4* gene in the mouse. The distinct phenotype observed in the *Sept4* null mice provides answers and clues to some of these remaining questions. In this report, we focus on the discovery of a septin-based circular structure in the spermatozoa of diverse mammals. Here, we reveal that the septin ring in the mouse spermatozoa is essential for cortical organization and intraflagellar transport, and demonstrate a critical role for the septin cytoskeleton in mammalian spermiogenesis and reproduction.

Results

Sept4 Is Essential for Male Fertility in Mice

To explore the postmitotic and postmeiotic roles of the septin cytoskeleton in vivo, we created mice lacking *Sept4*. The *Sept4* gene and its products are expressed mainly in postmitotic neural cells (Kinoshita et al., 2000) and postmeiotic male germ cells (Figure 1A). The targeting vector was designed to replace the entire coding exons 2–10 with a *neo* cassette to make a null allele (Figure 1B). The $Sept4^{+/-}$ and $Sept4^{-/-}$ mice were born at a rate close to the predicted Mendelian frequency. Elimination of the SEPT4 polypeptides in $Sept4^{-/-}$ tissues was confirmed (Figure 4 and not shown). The $Sept4^{-/-}$ mice had normal health without spontaneous development of malignancy (solid tumor and hematologic) until up to 10 months old ($n > 150$), except that males were completely sterile (Figure 1C). In contrast, $Sept4^{+/-}$ males and $Sept4^{-/-}$ females were fertile and produced normal-size litters. There were no gross anatomical and histological differences in the seminal vesicles, prostates, testes and epididymides between $Sept4^{+/-}$ and $Sept4^{-/-}$ males (Figure 1C and Supplemental Figure S1). Thus, the sterility is not attributable to developmental abnormality in and/or immaturity of the male reproductive organs.

Sept4 Is Essential for Structural and Mechanical Integrity of the Mouse Spermatozoa

To elucidate defects underlying the male sterility, we compared mature spermatozoa collected from caudae epididymides of $Sept4^{+/-}$ and $Sept4^{-/-}$ mice by differential interference contrast (DIC) video microscopy. Strikingly, >90% of the *Sept4* null spermatozoa were either completely immotile or exhibited impaired flagellar movement (Figure 1C). None of *Sept4* null spermatozoa had a dark ring which separates the middle and principal pieces in normal spermatozoa (Figure 2A). Instead, each had a segment of narrow caliber in the corresponding region, many of which were sharply bent or broken (Figures 2A and 2B). In contrast, immature spermatozoa collected from $Sept4^{-/-}$ caput epididymis were neither bent nor broken (Figure 2B). Thus, it is likely that the structural fragility of *Sept4* null spermatozoa manifests when their flagella start moving after maturation in the cauda epididymis. As the number of spermatozoa in $Sept4^{-/-}$ vas deferens was within the normal range (Figure 1C), the $Sept4^{-/-}$ mice infertility is technically attributable not to oligozoospermia (low sperm concentration), but to terato-asthenospermia (defective sperm morphology and motility).

Septin Organization in Normal and *Sept4* Null Spermatozoa

To address the molecular basis underlying the structural and mechanical defects of the *Sept4* null spermatozoa, we examined the subcellular localization of SEPT4 and other septin subunits in normal spermatozoa. Immunocytochemistry and fluorescence microscopy analysis detected SEPT4 as a pair of dots beneath the plasma membrane between the middle and principal pieces (Figure 2C). The dots often appeared fused depending on the staining conditions. Three other septin subunits, SEPT1/6/7, colocalized to the SEPT4 dots (Figure 2C and Supplemental Figure S2), while Sept2/5/8/10/11/12 and the major cytoskeletal proteins, α-tubulin, β-actin, and vimentin, were not concentrated at the dots (data not shown). On the other hand, SEPT1/6/7 were delocalized and dispersed throughout the cytoplasm in *Sept4* null spermatozoa (Figure 2D and Supplemental Figure S2).

Defective Cortical Organization in *Sept4* Null Spermatozoa

Consistently, immuno-electron microscopy (immuno-EM) detected SEPT4 in a submembranous ring of high electron density which is known as the annulus (Figure 3A). By transmission electron microscopy (TEM), the diameter of the annulus in $Sept4^{+}$ spermatozoa was 0.58 ± 0.09 μm ($n = 38$), and the axonemal 9+2 structure and the surrounding outer dense fibers were indistinguishable between $Sept4^{+}$ and *Sept4* null spermatozoa (Figure 3B). The annulus maintained this constant diameter with or without rudimentary cytoplasm ("cytoplasmic droplet") around the middle piece (Figure 3C). The annulus is in closer proximity to the fibrous sheath than to mitochondria (Figures 3B and 3C). In *Sept4* null spermatozoa, however, the annulus was never found, and the fibrous sheath often failed to cover a proximal segment of the principal piece (Figure 3B). The defects of cortical organization between mitochondria and the fibrous sheath correspond to the narrow segment observed by DIC microscopy (Figure 2A). Thus, we conclude that SEPT1/4/6/7 form the major structural basis of the annulus, which fails to organize in the absence of the SEPT4 subunit. This situation is reminiscent of the yeast septin ring which is disorganized by deletion of any one of the five septin subunits (Frazier et al., 1998). Taken together, we conclude that genetic loss of *Sept4* results in segmental defects in cortical organization, and that the local cortical defects are primarily responsible for the severe fragility of *Sept4* null spermatozoa.

Proteomic Changes in the $Sept4^{-/-}$ Testis

To study proteomic changes accompanying the genetic loss of *Sept4*, we compared protein expression profiles of $Sept4^{+/+}$ and $Sept4^{-/-}$ testes by immunoblot. All the *Sept4*-derived polypeptides detected by the H5C2U antibody in the $Sept4^{+/+}$ testis extract were absent in

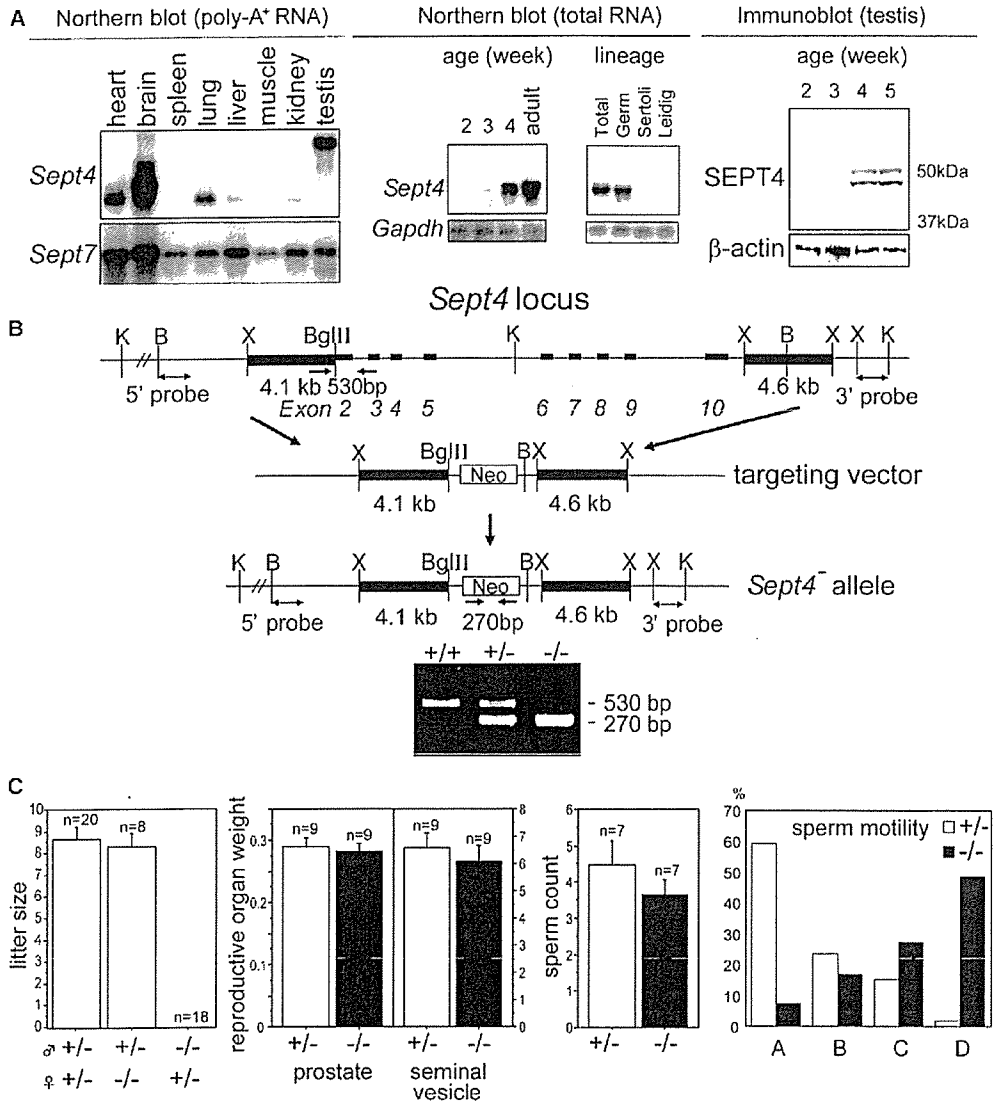

Figure 1. Loss of *Sept4* Abolishes Male Fertility in Mice

(A) Left: Tissue-specific expression of the mouse *Sept4* gene in comparison with the ubiquitous expression of *Sept7*. Each lane contained 2 μg poly A+ RNA. Middle: Haploid germ cell-specific expression of *Sept4* in mature testis. Each lane contained 20 μg total RNA. Right: Two SEPT4 isoforms of approximately 54 and 48 kDa appeared in 4-week-old testes following the increase in mRNA expression.

(B) Targeted disruption of *Sept4*. Top: A partial map of the mouse *Sept4* locus and diagrams showing the targeting strategy. Southern blot genotyping was done with indicated probes (data not shown). Bottom: Genotyping with the two sets of PCR primers shown in the above diagram.

(C) Complete sterility of the *Sept4*$^{-/-}$ male mice. From left to right: The *Sept4*$^{-/-}$ males never had offspring after successful matings with vaginal plugs. *Sept4*$^{-/-}$ males had mature reproductive organs, shown by an index of organ weight (in mg) per body weight (in g). There was no statistically significant difference in the number of spermatozoa ($\times 10^6$) collected from *Sept4*$^{+/-}$ and *Sept4*$^{-/-}$ vas deferens. Motility of spermatozoa derived from *Sept4*$^{+/-}$ and *Sept4*$^{-/-}$ mice was scored by the WHO classification; A, fast propulsion with straight trajectory, B, slow propulsion and/or tortuous trajectory, C, movement without propulsion, D, no movement (n = 410). (Supplemental movies are available at http://sentan1.hmro.med.kyoto-u.ac.jp/~top/teams/index_m_kinoshita_e.html.)

that of *Sept4*$^{-/-}$ (Figure 4). In addition to the 54 kDa and 48 kDa (cytoskeletal) isoforms of SEPT4, this antibody recognized shorter products including the 46 kDa ("mitochondrial") isoform (Takahashi et al., 2003). However, this and other SEPT4 antibodies never recognizably labeled mitochondria in normal spermatozoa (Figures 2C and 3A) and in the brain (Kinoshita et al., 2000). Thus, most of the 46 kDa isoform may not be targeted to mitochondria in vivo under normal conditions. We have not been able to confirm by RT-PCR and sequencing whether the mouse *Sept4* gene generates an ortholog of the human 32 kDa (mitochondrial, proapo-

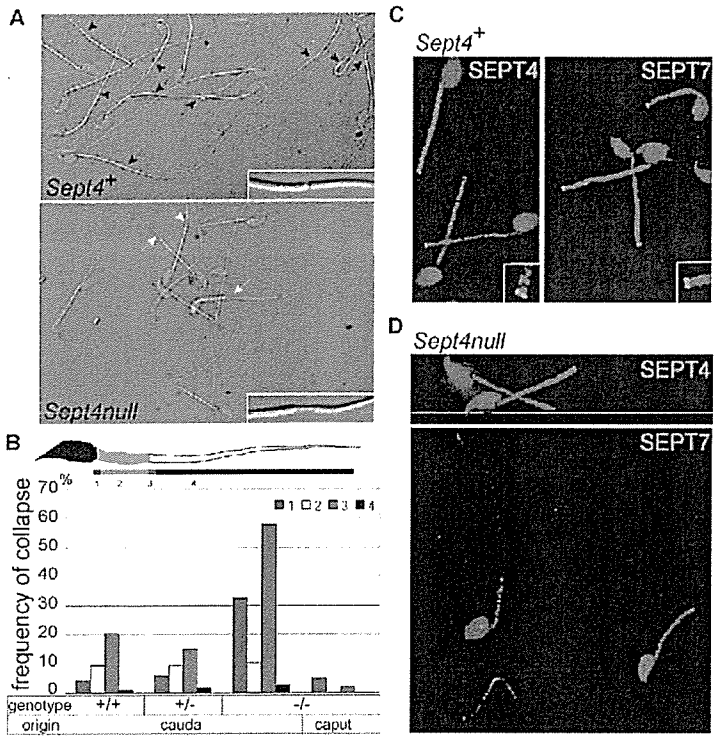

Figure 2. *Sept4* Null Spermatozoa Collapse at the Narrow Segment between the Middle and Principal Pieces

(A) DIC images of spermatozoa derived from *Sept4*$^{+/-}$ and *Sept4*$^{-/-}$ mice. Top: The middle and principal pieces of the *Sept4*$^{+}$ spermatozoa were clearly demarcated by a dark ring (black arrows and insert). Bottom: Instead of the dark ring, *Sept4* null spermatozoa had an ~5-μm-long segment with a smaller diameter in the corresponding region (white arrows and insert), most of which were sharply bent or broken (red arrows). The junction between the head and middle piece, termed the connecting piece, was also fragile (blue arrow).

(B) The local fragility was scored by the frequency of collapse (bend and break). *Sept4* null spermatozoa collected from cauda epididymis were bent most frequently near the border between the middle and principal pieces (zone 3, red), followed by the head-middle piece junction (zone 1, blue). The border between the middle and principal pieces is inherently fragile even in normal spermatozoa. In contrast, immature *Sept4* null spermatozoa collected from caput epididymis had minimal defects, indicating that the collapse occurs at the last stage of sperm maturation. n = 2000.

(C) Immunofluorescence images of spermatozoa collected from *Sept4*$^{+/-}$ cauda epididymis showing subcellular localization of SEPT4 or SEPT7 (green), nuclear DNA (blue), and vital staining for mitochondria (red). The two septins colocalized near the dark ring shown in (A), where SEPT1 and SEPT6 also colocalized (Supplemental Figure S2).

(D) Immunofluorescence images of spermatozoa collected from *Sept4*$^{-/-}$ cauda epididymis showing complete loss of the SEPT4 signal and delocalization of SEPT7. Color coding is the same as in (C). Neither SEPT1 nor SEPT6 localized near the middle-principal piece border (Supplemental Figure S2).

ptotic) polypeptide called ARTS (data not shown). Antibodies that recognize the putaive proapoptotic *Sept4* product in the mouse tissues have not been available.

Expression levels of the other septin subunits were comparable or slightly reduced in *Sept4*$^{-/-}$ testes (Figure 4). It has previously been known in other systems that loss of a septin subunit can affect the stability of other subunits in the same complex (Fares et al., 1995; Dent et al., 2002; Kinoshita et al., 2002). Although expression of microtubule and associated proteins (α-tubulin, dynein intermediate chain, dynactin, kinesins) remained unchanged, β-actin was consistently and significantly reduced in *Sept4*$^{-/-}$ testes. These results are concordant with the disorganization of actin bundles after RNAi-mediated septin depletion in tissue culture cells (Kinoshita et al., 2002). In addition, we consistently observed a reduction of a mitochondrial respiratory enzyme (and an apoptosis mediator) cytochrome C in *Sept4*$^{-/-}$ testes, while another enzyme cytochrome oxidase subunit IV (COX IV) did not change significantly. Although the mechanism and significance of these unexpected changes are currently unknown, genetic loss of *Sept4* appears to have a considerable impact on the testis/sperm proteome.

Low ATP Consumption and Impaired Microtubule Motor Activity in *Sept4* Null Spermatozoa

Next, we explored abnormalities responsible for the poor motility of *Sept4* null spermatozoa. The mechanical defects may be due not only to the structural defects but also to low viability or inert energy metabolism. As a common index of viability and energy metabolism, we measured the ATP level of mature spermatozoa immediately after collection from *Sept4*$^{+/-}$ and *Sept4*$^{-/-}$ caudae epididymides. Unexpectedly, *Sept4* null spermatozoa contained far more ATP than normal spermatozoa (2.3 versus 3.6 × 10^8 ATP molecules per *Sept4*$^{+}$ and *Sept4* null spermatozoon, respectively) (Figure 5A). After incubation in TYH medium at 37°C for 1 hr, the steady-state ATP level of *Sept4*$^{+}$ spermatozoa was reduced by 59%, whereas that of *Sept4* null increased by 3%. The net ATP consumption during the 1 hr incubation, which was estimated by blocking mitochondrial oxidative phosphorylation with cyanide, was 1.8 and 1.1 (×10^8 ATP/spermatozoon/hr), respectively. We conclude that *Sept4* null spermatozoa are viable and able to generate ATP, but are unable to utilize ATP robustly.

The low ATP consumption and motility of *Sept4* null spermatozoa indicate a severe functional defect in the major flagellar motor, dynein ATPase. However, we found neither loss nor mislocalization of dynein (tested only for the intermediate chain) in *Sept4* null spermatozoa by immunoblot and immunofluorescence (Figure 4 and data not shown). Thus, we speculate that axonemal deformity caused by the sharp bend may hamper the coordinated sliding motion of the tubulin-dynein crossbridges. Since this hypothesis alone cannot ac-

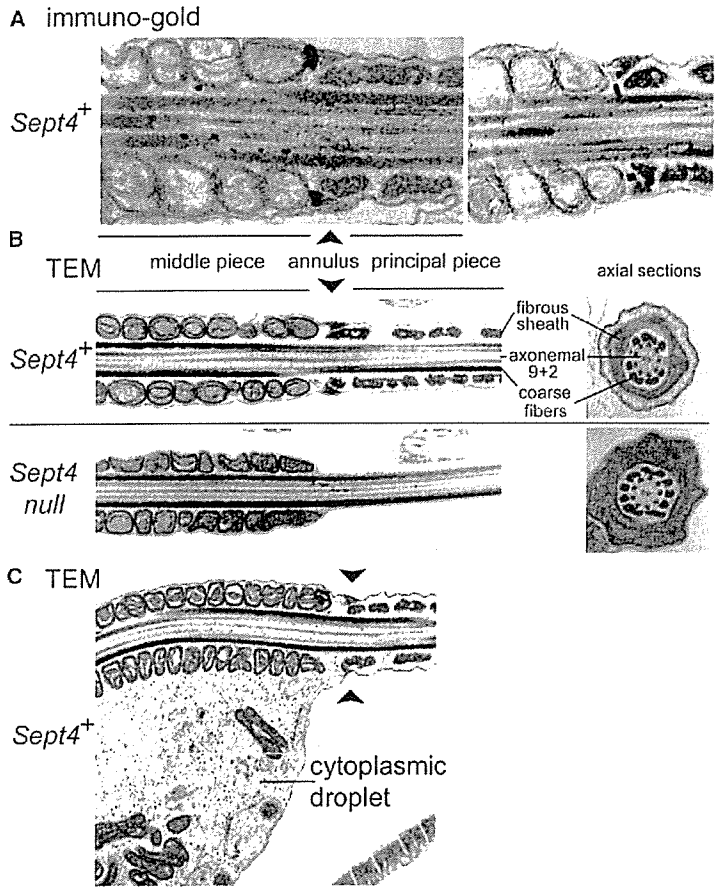

Figure 3. The Annulus, a Septin-Based Cortical Ring, Is Not assembled in *Sept4* Null Spermatozoa

(A) Immuno-gold labeling for SEPT4 in *Sept4*$^+$ mouse spermatozoa (sagittal sections, head to the left). SEPT4 (labeled with large black dots) consistently localized to the annulus which is seen as a pair of electron-dense, wedge-shaped structures beneath the plasma membrane (arrowhead at the bottom).

(B) TEM images of *Sept4*$^+$ and *Sept4* null spermatozoa in sagittal (left panels) and axial (right panels) sections. Top, left: Annulus (arrowhead at the top) in a *Sept4*$^+$ spermatozoon is seen as a distinct ring intervening in the mitochondrial array (on the left) and fibrous sheath (on the right). Top, right: An axial section of a *Sept4*$^+$ spermatozoon at the principal piece shows the fibrous sheath, coarse fibers, and axonemal 9+2 structure. Bottom, left: The annulus is completely lost in a *Sept4* null spermatozoon, leaving a thin segment without mitochondria or a fibrous sheath at the cortex. Bottom, right: An axial section of a *Sept4* null spermatozoon at the middle piece shows ultrastructurally normal coarse fibers and axonemal 9+2 structure.

(C) A TEM image of a sagittally sectioned *Sept4*$^+$ spermatozoon with a cytoplasmic droplet around the middle piece. The annulus appears to anchor the plasma membrane to the proximal end of the fibrous sheath.

count for the immotility of straight *Sept4* null spermatozoa, we explored other factors that affect ATP consumption in *Sept4* null spermatozoa. We examined the status of kinesins, another class of motor proteins which are required for intraflagellar transport along the axoneme toward its tip (Scholey, 2003). In *Sept4*$^+$ spermatozoa, a pan-kinesin antibody SUK4 gave punctate labeling along the distal axoneme and a larger spot near the centrosome in the neck region (Figure 5B). On the other hand, punctate signals for kinesins clustered near the narrow segment of *Sept4* null spermatozoa irrespective of the presence of a sharp bend. These data indicate that kinesin-mediated intraflagellar transport somehow stalls beneath the defective cortex in the *Sept4* null spermatozoa, despite an apparently intact axonemal 9+2 structure (Figure 3B). Since kinesin-mediated intraflagellar transport is essential for microtubule stability and dynein activation (Carvalho et al., 2004), its failure to progress farther than the narrow segment in *Sept4*-null spermatozoa might affect downstream microtubule organization and/or dynein motor activity. Taken together, we currently hypothesize that the dynein motor in *Sept4* null spermatozoa cannot fully utilize ATP, perhaps because the defective intraflagellar transport affects its activation, and/or the sharp bend in the axoneme prevents its sliding motion.

The *Sept4* Null Spermatozoon Carries a Normal Haploid Genome

To test possible meiotic defects in *Sept4*$^{-/-}$ mice, we asked whether their sterility can be rescued by in vitro fertilization techniques. The sterility of *Sept4*$^{-/-}$ mice was barely rescued by in vitro fertilization (Supplemental Table S3). On the other hand, intracytoplasmic injection of *Sept4* null sperm nuclei (ICSI) was able to fertilize oocytes, some of which developed normally to birth (Supplemental Table S4 and Supplemental Figure S4). These and above data indicate that each *Sept4* null spermatozoon carries an intact haploid genome as a result of normal spermatogenesis, whereas the structural and mechanical defects developed during spermiogenesis and subsequent maturation steps prevent their propulsion and entry into oocytes.

Defective Annulus/Septin Ring Organization in Human Asthenospermia

Thus far, we have demonstrated in mice that defective sperm motility accompanies disorganization of the sperm cortex and annulus. Since sperm morphology shows considerable interspecies diversity, we tested whether septins also comprise the annulus in other mammals. Among our septin antibodies, those against SEPT7 consistently labeled the human and bovine annulus

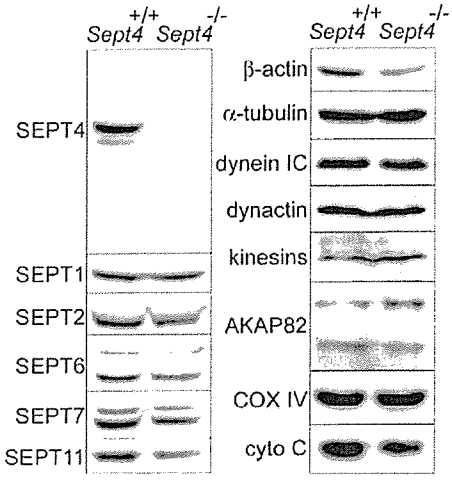

Figure 4. Genetic Loss of *Sept4* Causes Proteomic Changes in the Testis

Immunoblot analysis of extracts from *Sept4*$^{+/+}$ and *Sept4*$^{-/-}$ testes. All the bands for SEPT4 were absent in the *Sept4*$^{-/-}$ testis, which established specificity of the antibody H5C2U used throughout this study. In the *Sept4*$^{-/-}$ testis, SEPT1/2/6/7/11, β-actin and cytochrome C (cyto C) were slightly reduced; α-tubulin, dynein intermediate chain, kinesins, a fibrous sheath protein, AKAP82, and mitochondrial cytochrome oxidase subunit IV (COX IV) were unchanged. Each lane contained 100 μg protein. Consistent results were obtained in two or three experiments.

most intensely, followed by those against SEPT1/4/6 (Figure 6A and Supplemental Figure S3; and data not shown). Thus, the role for the septin cytoskeleton in annulus organization seems conserved throughout mammalian evolution.

Finally, we asked whether loss of the annulus/septin ring is involved in human male infertility. Frozen semen samples derived from human male infertility patients were processed for immunofluorescence analysis using the SEPT7 antibody. Among 22 infertile sperm samples of various clinical categories, three samples were devoid of the septin ring and annulus as determined by immunofluorescence and TEM, respectively (Figure 6 and data not shown). Interestingly, each case had been clinically diagnosed as idiopathic asthenospermia without oligozoospermia. Teratozoospermia as seen in the *Sept4* null mice (e.g., segmental narrowing and bend) was not evident in these cases. On the other hand, asthenospermia seems to correlate with the loss of the annulus/septin ring in humans. Considering the high incidence, disorganization of the annulus/septin ring may be a common phenotype that occurs in mammalian asthenospermia of various etiology.

Discussion

This study revealed a previously uncharacterized function of the septin cytoskeleton in a postmeiotic, terminally differentiated cell. The genetic loss of *Sept4* caused disorganization of the annulus and adjacent cortex, which resulted in fragility and immotility of the spermatozoa. Thus, septin-based organization of the annulus is a requisite for the structural and mechanical integrity of the mammalian spermatozoa.

Annulus as a Septin Ring

Despite the interspecies diversity of sperm morphology, the septin subunits were consistently found in the annulus of spermatozoa from three distant mammalian species. The unique property of septin hetero-oligomers to assemble in vitro as circular bundles of 0.51 ± 0.07 μm in diameter (Kinoshita et al., 2002) seems suitable for organization of the annulus, which exhibits both a similar shape and size (0.58 ± 0.09 μm). The loss of the annulus and the adjacent cortex in *Sept4* null spermatozoa indicates that the annulus/septin ring may serve as a cortical scaffold to organize the fibrous sheath immediately distal to the mitochondrial array. In the case of contractile ring assembly during metazoan cytokinesis, septins are circularly organized beneath the equatorial plasma membrane by anillin, a pleckstrin homology domain protein that interacts with both septins and lipid (Oegema et al., 2000; Kinoshita et al., 2002). Since anillin is absent in the annulus (data not shown), the septins are targeted beneath the plasma membrane by another mechanism. The lipid binding property of SEPT4 (Zhang et al., 1999) might serve for this purpose.

The annulus has been hypothesized to function as a diffusion barrier between the middle and principal pieces for membrane-bound sperm proteins such as rat glycoprotein CE9 (an ortholog of mouse emmprin and human CD147) (Cesario and Bartles, 1994). The yeast septin mutants helped establish the concept that the septin ring is the diffusion barrier between the mother and bud membrane compartments (Barral et al., 2000; Takizawa et al., 2000). Likewise, the *Sept4* null spermatozoa should serve as a means to test the significance of annulus/septin-ring-dependent compartmentation of emmprin and other cortical molecules.

Other unanswered questions related to the annulus include the mechanism by which the annulus/septin ring is positioned and assembled during normal spermiogenesis, and the mechanism by which the adjacent cortex is lost in the absence of a septin subunit. Since the septin cytoskeleton also plays a role in *Drosophila* spermatogenesis (Hime et al., 1996), this unique cytoskeleton may be universally required for male meiosis in metazoa. Future studies with other species and approaches should further clarify septin-mediated processes in spermato/spermiogenesis.

Causal Link between Loss of *Sept4* and Immotility

The mechanism by which loss of *Sept4* and/or the cortical defects affect flagellar motility is still unclear. Although axonemal 9+2 structure in the *Sept4* null spermatozoa was normal at EM level, the excess ATP reserve indicates that the major ATPases such as dynein cannot utilize ATP for some reason. The simplest explanation would be that axonemal deformity, due to the sharp bend, mechanically prevents the axonemal sliding machinery. However, this mechanism alone cannot explain the immotility of *Sept4* null spermatozoa which do not exhibit this bend.

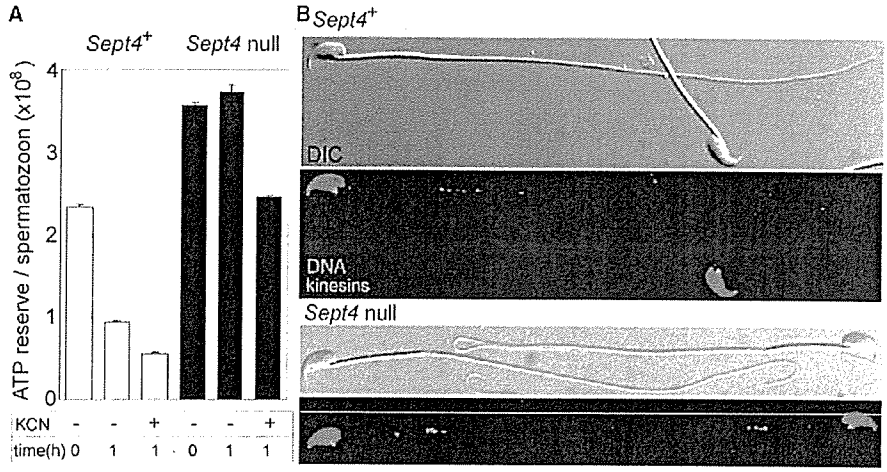

Figure 5. Reduced ATP Consumption and Defective Intraflagellar Transport in *Sept4* Null Spermatozoa

(A) ATP reserve and consumption of *Sept4*$^{+}$ and *Sept4* null spermatozoa. ATP content in mature spermatozoa immediately after collection from *Sept4*$^{+/-}$ and *Sept4*$^{-/-}$ cauda epididymis was measured by a luciferase method (time 0). During subsequent incubation of *Sept4*$^{+}$ spermatozoa, flagellar movement and ATP consumption increased. Consequently, the ATP reserve in *Sept4*$^{+}$ spermatozoa was markedly reduced after 1 hr. In contrast, this did not occur in *Sept4* null spermatozoa. The net ATP consumption was estimated by inhibiting ATP production by adding 5 mM KCN to the media. The measurement was triplicated and divided by the number of spermatozoa.

(B) Aberrant kinesin localization in *Sept4* null spermatozoa (DIC and immunofluorescence images). Top: In each *Sept4*$^{+}$ spermatozoon, a pan-kinesin antibody, SUK4, gave punctate labeling throughout the axoneme and a larger dot at the head-middle piece junction known as the connecting piece. The larger dot is likely to correspond to centrosomal kinesins. Bottom: In *Sept4* null spermatozoa, the punctate signals for kinesins were concentrated near the narrow segment irrespective of the presence of a bend. The signal intensity and localization of the dot at the connecting piece appeared unaffected. DNA: blue, kinesins: green.

A clue may come from the accumulation of kinesins near the narrow segment of *Sept4* null spermatozoa, because the failure of kinesin motors to progress beyond this segment indicates local defects in the axoneme. Perhaps SEPT4 and/or the normal cortex are required for proper organization of the core axonemal structure. This hypothesis may be supported by the fact that depletion of a septin subunit affects microtubule organization in tissue culture cells (Surka et al., 2002; Nagata et al., 2003). Reciprocally, defects in kinesin-mediated intraflagellar transport may affect both microtubule stability and dynein activation (Carvalho et al., 2004). Thus, a subtle defect in the axoneme might initiate a vicious cycle affecting the two microtubule motor proteins. The nature of the hypothetical axonemal defects in the *Sept4* null spermatozoa is an intriguing subject for future studies.

Association between Annulus Disorganization and Asthenospermia in Humans

About 15% of human couples remain childless due to infertility, and roughly half of the cases are attributable to male infertility. Although many genetic factors are likely to underlie most cases of idiopathic male infertility, few responsible genes have been identified (Matzuk and Lamb, 2002). Although this common syndrome (incidence: 1 in ~200 males) consists of heterogeneous etiology, further classification has not been enabled partly due to absence of appropriate markers.

This study revealed defective annulus/septin ring organization in 20% of infertility patients with idiopathic asthenospermia syndrome without oligozoospermia (n = 15). We have not explored genetic defects in these patients lacking the annulus, because it is unlikely that septin gene defects are so common. Perhaps defects in a certain class of molecules involved in spermiogenesis affects annulus/septin ring organization. If a correlation between loss of annulus and mechanical defects in spermatozoa is established in larger-scale clinical studies, it should serve as a diagnostic criterion to classify asthenospermia syndrome.

Addressing Other Questions with *Sept4*$^{-/-}$ Mice

Besides asthenospermia syndrome, human *Sept4* is also implicated in leukemogenesis with its proapoptotic product (Larisch et al., 2000; Elhasid et al., 2004). As yet, we have not obtained positive data to support the possible involvement of mouse *Sept4* in leukemogenesis as a tumor-suppressor or a proapoptotic factor. For instance, the *Sept4*$^{-/-}$ mice have never developed spontaneous malignancy at recognizable gravity and frequency, and the *Sept4*$^{-/-}$ testes exhibited no histological abnormalities (Supplemental Figure S1). Perhaps loss of *Sept4* is either negligible or compensated for in mouse tissues. We should note that an opposite possibility of *Sept4* as an oncogene has not been excluded either. Challenging *Sept4*$^{-/-}$ mice with carcinogens or establishing *Sept4*$^{-/-}$ mice with a cancer-prone genetic background may reveal additional roles for *Sept4* during tumorigenesis/leukemogenesis.

Human Sept4 is also implicated in the neuropathology of Alzheimer's disease (Kinoshita et al., 1998) and

A

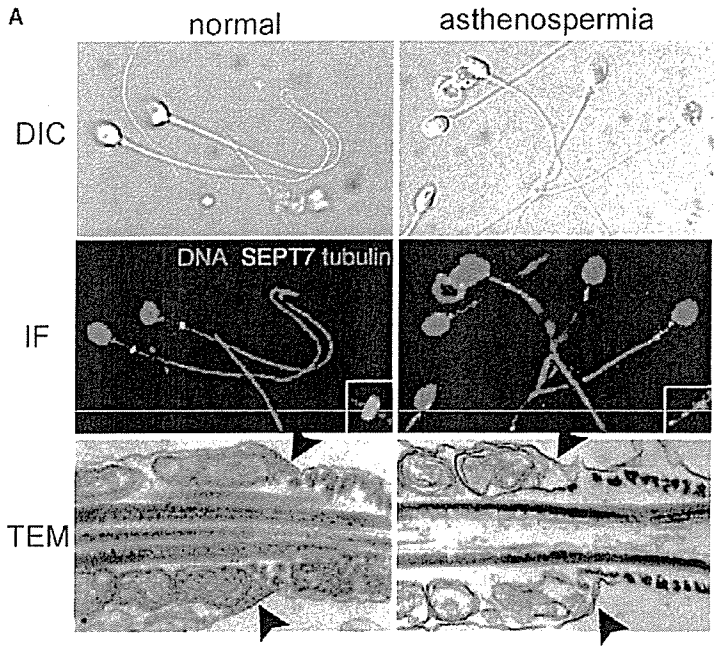

Figure 6. Septin Disorganization and Loss of the Annulus in a Subset of Human Asthenospermia

(A) DIC, immunofluorescence, and TEM images (sagittal section, head to the left) of human spermatozoa derived from a fertile individual (labeled as normal) and an infertile patient with defective sperm motility (labeled as asthenospermia). In the middle panel, samples were labeled for nuclear DNA (blue), SEPT7 (green), and α-tubulin (red). As seen in the mouse and bovine spermatozoa (Figure 2C and Supplemental Figure S3), the SEPT7 antibody specifically labeled the annulus in the human spermatozoa (arrowheads in TEM). Incubation of the normal sperm samples at room temperature overnight did not affect the signal intensity and localization. In contrast, neither septin ring (by IF) nor the annulus (by TEM) was organized in the samples derived from three patients with asthenospermia syndrome (right panels and not shown).

(B) Summary of the screening for annulus/septin ring defects in humans. See text for details.

B

Summary of the clinical cases	n	annulus (-)
normal	8	0
asthenospermia		
without oligozoospermia	15	3
with oligozoospermia	5	0
necrozoospermia	2	0

Parkinson's disease (Ihara et al., 2003). Since parkin gene mutants generated in *Drosophila* exhibit abnormalities in mitochondrial morphology and spermatogenesis (Greene et al., 2003), players and/or pathways may be shared in these processes. The *Sept4*$^{-/-}$ mice established in this study should provide an in vivo model system to address many of the questions that remain in septin biology and beyond.

Experimental Procedures

Generation of *Sept4*$^{-/-}$ Mice and Animal Handling

We isolated, mapped, and sequenced a BAC clone containing ~26 kb mouse genomic DNA for *Sept4*. We constructed a targeting vector by subcloning the fragments into the 38LoxPNeo plasmid (a modified version of pGT-N38 from New England Biolabs), which is designed to replace exons 2–10 containing the entire coding region with a *neo* cassette. We electroporated 129Sv/J embryonic stem cells with the linearized targeting vector and subjected them to neomycin selection. We identified *Sept4* targeted clones by Southern blot hybridization with the probes, injected these cells into blastocysts, and mated chimeric offspring with C57BL/6J mice. We determined their genotype by PCR (Figure 1B) and intercrossed *Sept4*$^{+/-}$ F1 mice to produce *Sept4*$^{-/-}$ mice. For IVF and ICSI, we used B6D2F1 (B57BL/6 × DBA/2), C57BL/6, and ICR mice of 2- to 4-months old. The protocol of animal handling and treatment was reviewed and approved by the Animal Care and Use Committee of Kyoto University.

Northern Blot Analysis

We homogenized tissues from adult C57BL/6 mice or fractionated testicular cells in RNAzol B (Tel-Test Inc.), extracted total RNA, and performed RNA blot as described (Tanaka et al., 2004). We used the coding regions of the longest form of mouse *Sept4* and human *Sept7* cDNA to prepare ^{32}P-labeled probes by a random primer method. After hybridization, we washed the filters stringently (twice in 0.3× SSC plus 0.1% SDS at 60°C) and detected the signals with an imaging plate (Fuji Film). As a loading control, we reprobed the same filters for the glyceraldehyde-3-phosphate dehydrogenase (GAPDH) gene.

Antibodies

We raised rabbit antisera against, and affinity-purified with, a synthetic oligopeptide H5C2 (CMLHKIQRQMKETH) corresponding to the carboxyl terminus of the major isoforms of mouse SEPT4. The purified antibody also recognized human and bovine orthologs (Figure 6A and Supplemental Figure S3; and data not shown). The other antibodies were either published (SEPT2/5/6/7, Kinoshita et al., 2000, 2002), unpublished (SEPT1/8/9/10/11/12), or purchased (anti-α-tubulin from Abcam; anti-dynein intermediate chain from Chemicon; anti-vimentin and anti-β-actin from Sigma; anti-AKAP82, anti-dynactin, and anti-cytochrome C from BD Transduction Laboratories; and anti-pan-kinesin SUK4 from Cytoskeleton).

Fluorescence and Electron Microscopy

Spermatozoa with or without mitochondrial vital staining (Mito-Tracker Red CMXRos, Molecular Probes) were observed alive, or smeared on glass coverslips, briefly dried, fixed with 3.7% formaldehyde in PBS then permeabilized with 0.1% Triton X-100 in PBS,

or treated with cold methanol. Staining, fluorescence microscopy, and deconvolution were done as described (Kinoshita et al., 1997). For TEM, spermatozoa were fixed with 2% glutaraldehyde in 0.1 M phosphate buffer, embedded in 1% agar, stained with 2% OsO_4 for 1 hr, dehydrated by graded ethanol, and embedded in epoxy resin (ERL4206, TAAB). We cut ultrathin sections, stained them with 1% uranyl acetate and lead citrate, and observed them with a transmission electron microscope (H7100, Hitachi). For immuno-electron microscopy, we used a pre-embedding immunogold labeling method (Kinoshita et al., 2000).

Testis Histochemistry and Analysis of Apoptotic Cells

We fixed testes in 4% formalin neutral buffer solution and made 6-μm-thick paraffin sections. We stained the sections with hematoxylin and eosin. We detected apoptotic cells by TUNEL assay with ApopTag peroxidase kit (Invitrogen).

Collection and Examination of Spermatozoa, IVF, and ICSI

We collected spermatozoa from the caudae epididymides of 12–20 week old mice and suspended them in HTF medium pre-equilibrated with 5% CO_2 at 37°C (Toyoda et al., 1971). We carried out IVF and ICSI essentially as described (Kimura and Yanagimachi, 1995; Tanaka et al., 2004). We counted oocytes with two distinct pronuclei and a conspicuous second polar body as fertilized normally. Bovine sperm were a gift from Kyoto Prefectural Livestock and Poultry Research Institute.

ATP Measurement

We used the CellTiter-Glo luminescent cell viability assay system (Promega). We made triplicated measurements of sperm suspensions (50 μl in TYH) lysed with 50 μl reagent in each well of a 96-well plate using plate reader ARVO (Wallac). We made a standard curve of ATP versus relative luminescence unit, and measured the sample within its linearity range (0–10 nM).

Human Materials

Human sperm samples were collected under signed informed consent at Kyoto University Hospital. Our clinical study has been approved by the ethics committee of Kyoto University.

Supplemental Data

Supplemental Data associated with this article can be found online at http://www.developmentalcell.com/cgi/content/full/8/2/343/DC1/. The supplemental data set contains four supplemental figures and five supplemental tables.

Acknowledgments

We thank N. Watanabe and Y. Kaziro for encouragement, H. Kimura, H. Watanabe, and H. Nakabayashi for technical assistance, and J. Monypenny for editing the manuscript. This study was supported in part by Special Coordination Funds for Promoting Science and Technology from the Ministry of Education, Culture, Sports, Science and Technology of Japan, PRESTO from Japan Science and Technology Agency (to M.K.), and a postdoctoral fellowship from Japan Society for Promotion of Science (to M.I.). The authors declare that they have no competing financial interests.

Received: July 30, 2004
Revised: September 24, 2004
Accepted: October 14, 2004
Published: February 28, 2005

References

Adam, J.C., Pringle, J.R., and Peifer, M. (2000). Evidence for functional differentiation among Drosophila septins in cytokinesis and cellularization. Mol. Biol. Cell *11*, 3123–3135.

Barral, Y., Mermall, V., Mooseker, M.S., and Snyder, M. (2000). Compartmentalization of the cell cortex by septins is required for maintenance of cell polarity in yeast. Mol. Cell *5*, 841–851.

Beites, C.L., Xie, H., Bowser, R., and Trimble, W.S. (1999). The septin CDCrel-1 binds syntaxin and inhibits exocytosis. Nat. Neurosci. *2*, 434–439.

Byers, B., and Goetsch, L. (1976). A highly ordered ring of membrane-associated filaments in budding yeast. J. Cell Biol. *69*, 717–721.

Carvalho, P., Gupta, M.L., Jr., Hoyt, M.A., and Pellman, D. (2004). Cell cycle control of kinesin-mediated transport of Bik1 (CLIP-170) regulates microtubule stability and dynein activation. Dev. Cell *6*, 815–829.

Cesario, M.M., and Bartles, J.R. (1994). Compartmentalization, processing and redistribution of the plasma membrane protein CE9 on rodent spermatozoa. Relationship of the annulus to domain boundaries in the plasma membrane of the tail. J. Cell Sci. *107*, 561–570.

Dent, J., Kato, K., Peng, X.R., Martinez, C., Cattaneo, M., Poujol, C., Nurden, P., Nurden, A., Trimble, W.S., and Ware, J. (2002). A prototypic platelet septin and its participation in secretion. Proc. Natl. Acad. Sci. USA *99*, 3064–3069.

Elhasid, R., Sahar, D., Merling, A., Zivony, Y., Rotem, A., Ben-Arush, M., Izraeli, S., Bercovich, D., and Larisch, S. (2004). Mitochondrial pro-apoptotic ARTS protein is lost in the majority of acute lymphoblastic leukemia patients. Oncogene *23*, 5468–5475.

Fares, H., Peifer, M., and Pringle, J.R. (1995). Localization and possible functions of Drosophila septins. Mol. Biol. Cell *6*, 1843–1859.

Finger, F.P., Kopish, K.R., and White, J.G. (2003). A role for septins in cellular and axonal migration in C. elegans. Dev. Biol. *261*, 220–234.

Field, C.M., and Kellogg, D. (1999). Septins, cytoskeletal polymers or signalling GTPases? Trends Cell Biol. *9*, 387–394.

Frazier, J.A., Wong, M.L., Longtine, M.S., Pringle, J.R., Mann, M., Mitchison, T.J., and Field, C. (1998). Polymerization of purified yeast septins: evidence that organized filament arrays may not be required for septin function. J. Cell Biol. *143*, 737–749.

Gladfelter, A.S., Pringle, J.R., and Lew, D.J. (2001). The septin cortex at the yeast mother-bud neck. Curr. Opin. Microbiol. *4*, 681–689.

Greene, J.C., Whitworth, A.J., Kuo, I., Andrews, L.A., Feany, M.B., and Pallanck, L.J. (2003). Mitochondrial pathology and apoptotic muscle degeneration in Drosophila parkin mutants. Proc. Natl. Acad. Sci. USA *100*, 4078–4083.

Hime, G.R., Brill, J.A., and Fuller, M.T. (1996). Assembly of ring canals in the male germ line from structural components of the contractile ring. J. Cell Sci. *109*, 2779–2788.

Ihara, M., Tomimoto, H., Kitayama, H., Morioka, Y., Akiguchi, I., Shibasaki, H., Noda, M., and Kinoshita, M. (2003). Association of the cytoskeletal GTP-binding protein Sept4/H5 with cytoplasmic inclusions found in Parkinson's disease and other synucleinopathies. J. Biol. Chem. *278*, 24095–24102.

Kimura, Y., and Yanagimachi, R. (1995). Intracytoplasmic sperm injection in the mouse. Biol. Reprod. *52*, 709–720.

Kinoshita, M., Kumar, S., Mizoguchi, A., Ide, C., Kinoshita, A., Haraguchi, T., Hiraoka, Y., and Noda, M. (1997). Nedd5, a mammalian septin, is a novel cytoskeletal component interacting with actin-based structures. Genes Dev. *11*, 1535–1547.

Kinoshita, A., Kinoshita, M., Akiyama, H., Tomimoto, H., Kumar, S., Noda, M., and Kimura, J. (1998). Identification of septins in the neurofibrillary tangles in Alzheimer's disease. Am. J. Pathol. *15*, 1551–1560.

Kinoshita, A., Noda, M., and Kinoshita, M. (2000). Differential localization of septins in the mouse brain. J. Comp. Neurol. *428*, 223–239.

Kinoshita, M., Field, C.M., Coughlin, M.L., Straight, A.F., and Mitchison, T.J. (2002). Self- and actin-templated assembly of mammalian septins. Dev. Cell *3*, 791–802.

Kusch, J., Meyer, A., Snyder, M.P., and Barral, Y. (2002). Microtubule capture by the cleavage apparatus is required for proper spindle positioning in yeast. Genes Dev. *16*, 1627–1639.

Larisch, S., Yi, Y., Lotan, R., Kerner, H., Eimerl, S., Tony Parks, W., Gottfried, Y., Birkey Reffey, S., de Caestecker, M.P., Danielpour, D., et al. (2000). A novel mitochondrial septin-like protein, ARTS, medi-

ates apoptosis dependent on its P-loop motif. Nat. Cell Biol. *2*, 915–921.

Matzuk, M.M., and Lamb, D.J. (2002). Genetic dissection of mammalian fertility pathways. Nat. Med. Suppl., *2*, S33–S40.

Nagata, K., Kawajiri, A., Matsui, S., Takagishi, M., Shiromizu, T., Saitoh, N., Izawa, I., Kiyono, T., Itoh, T.J., Hotani, H., and Inagaki, M. (2003). Filament formation of MSF-A, a mammalian septin, in human mammary epithelial cells depends on interactions with microtubules. J. Biol. Chem. *278*, 18538–18543.

Neufeld, T.P., and Rubin, G.M. (1994). The Drosophila peanut gene is required for cytokinesis and encodes a protein similar to yeast putative bud neck filament proteins. Cell *77*, 371–379.

Nguyen, T.Q., Sawa, H., Okano, H., and White, J.G. (2000). The C. elegans septin genes, unc-59 and unc-61, are required for normal postembryonic cytokineses and morphogenesis but have no essential function in embryogenesis. J. Cell Sci. *113*, 3825–3837.

Oegema, K., Savoian, M.S., Mitchison, T.J., and Field, C.M. (2000). Functional analysis of a human homologue of the Drosophila actin binding protein anillin suggests a role in cytokinesis. J. Cell Biol. *150*, 539–552.

Scholey, J.M. (2003). Intraflagellar transport. Annu. Rev. Cell Dev. Biol. *19*, 423–443.

Surka, M.C., Tsang, C.W., and Trimble, W.S. (2002). The mammalian septin MSF localizes with microtubules and is required for completion of cytokinesis. Mol. Biol. Cell *13*, 3532–3545.

Takahashi, S., Inatome, R., Yamamura, H., and Yanagi, S. (2003). Isolation and expression of a novel mitochondrial septin that interacts with CRMP/CRAM in the developing neurones. Genes Cells *8*, 81–93.

Takizawa, P.A., DeRisi, J.L., Wilhelm, J.E., and Vale, R.D. (2000). Plasma membrane compartmentalization in yeast by messenger RNA transport and a septin diffusion barrier. Science *290*, 341–344.

Tanaka, M., Kijima, H., Itoh, J., Matsuda, T., and Tanaka, T. (2002). Impaired expression of a human septin family gene Bradeion inhibits the growth and tumorigenesis of colorectal cancer in vitro and in vivo. Cancer Gene Ther. *9*, 483–488.

Tanaka, H., Iguchi, N., Toyama, Y., Kitamura, K., Takahashi, T., Kaseda, K., Maekawa, M., and Nishimune, Y. (2004). Mice deficient in the axonemal protein Tektin-t exhibit male infertility and immotile-cilium syndrome due to impaired inner arm dynein function. Mol. Cell. Biol. *24*, 7958–7964.

Toyoda, Y., Yokoyama, M., and Hoshi, T. (1971). Studies on the fertilization of mouse eggs in vitro. Jpn. J. Anim. Reprod. *16*, 147–157.

Zhang, J., Kong, C., Xie, H., McPherson, P.S., Grinstein, S., and Trimble, W.S. (1999). Phosphatidylinositol polyphosphate binding to the mammalian septin H5 is modulated by GTP. Curr. Biol. *9*, 1458–1467.

THE JOURNAL OF BIOLOGICAL CHEMISTRY
Vol. 280, No. 18, Issue of May 6, pp. 17777–17785, 2005
Printed in U.S.A.

The Low Density Lipoprotein Receptor-related Protein (LRP) Is a Novel β-Secretase (BACE1) Substrate*

Received for publication, December 17, 2004, and in revised form, February 22, 2005
Published, JBC Papers in Press, March 4, 2005, DOI 10.1074/jbc.M414248200

Christine A. F. von Arnim‡§, Ayae Kinoshita‡§, Ithan D. Peltan‡, Michelle M. Tangredi‡, Lauren Herl‡, Bonny M. Lee‡, Robert Spoelgen‡, Tammy T. Hshieh‡, Sripriya Ranganathan¶, Frances D. Battey¶, Chun-Xiang Liu¶, Brian J. Bacskai‡, Sanja Sever‖, Michael C. Irizarry‡, Dudley K. Strickland¶, and Bradley T. Hyman‡**

From the ‡Alzheimer Disease Research Laboratory, Massachusetts General Hospital, Harvard Medical School, Charlestown, Massachusetts 02129, the ¶Departments of Surgery and Physiology, University of Maryland School of Medicine, Rockville, Maryland 20855, and the ‖Renal Unit, Massachusetts General Hospital, Harvard Medical School, Charlestown, Massachusetts 02129

BACE is a transmembrane protease with β-secretase activity that cleaves the amyloid precursor protein (APP). After BACE cleavage, APP becomes a substrate for γ-secretase, leading to release of amyloid-β peptide (Aβ), which accumulates in senile plaques in Alzheimer disease. APP and BACE are co-internalized from the cell surface to early endosomes. APP is also known to interact at the cell surface and be internalized by the low density lipoprotein receptor-related protein (LRP), a multifunctional endocytic and signaling receptor. Using a new fluorescence resonance energy transfer (FRET)-based assay of protein proximity, fluorescence lifetime imaging (FLIM), and co-immunoprecipitation we demonstrate that the light chain of LRP interacts with BACE on the cell surface in association with lipid rafts. Surprisingly, the BACE-LRP interaction leads to an increase in LRP C-terminal fragment, release of secreted LRP in the media and subsequent release of the LRP intracellular domain from the membrane. Taken together, these data suggest that there is a close interaction between BACE and LRP on the cell surface, and that LRP is a novel BACE substrate.

BACE[1] (β site of APP-cleaving enzyme) is a type I membrane-associated aspartyl protease that cleaves APP (1–4). Besides APP, the few BACE substrates that have been identified include the APP homologues APLP1 and -2 (5), P-selectin glycoprotein ligand-1 (PSGL-1), and a membrane-bound sialyltransferase (6). Post-translational processing of BACE involves *N*-glycosylation, removal of its prodomain by a furin-like protease, and further complex glycosylation (7–9). After glycosylation, BACE co-traffics with APP and is rapidly transported to the Golgi apparatus and distal secretory pathway (9). Measurable amounts of APP and BACE are present on the plasma membrane (10–12) and in lipid rafts (12–14). BACE and APP are internalized from the cell surface to early endosomes and cycle between the cell membrane and endosomes (10, 11, 15).

The low density lipoprotein receptor-related protein, LRP, is a type I integral membrane protein with a 515-kDa extracellular α-chain non-convalently bound to the 85 kDa membrane-spanning β-chain. It is also found on the cell surface and cycles between the cell membrane and endosomes. Multiple intracellular adaptor and scaffolding proteins bind the LRP 100 amino acid cytoplasmic tail (16, 17); its four extracellular binding domains mediate endocytosis of a wide array of ligands, including several of potential importance for Alzheimer disease pathophysiology: APP, apolipoprotein E and α_2-macroglobulin (16–18). The LRP ligand binding domains interact with KPI-containing forms of APP. In addition, an interaction between the C-terminal domain of APP and LRP, mediated by the cytoplasmic adaptor protein Fe65, impacts APP internalization (18–23). In addition to its role in endocytosis, LRP has an interesting pattern of proteolysis that parallels APP in some ways. Ectodomain shedding of LRP has been described (24) and proteolysis of LRP by matrix metalloproteases was recently reported (25); MT1-MMP also cleaves APP (26) and the postulated α-secretases of the ADAM family are also metalloproteinases. Furthermore, and as with APP, γ-secretase cleavage of LRP leads to release of the LRP intracellular domain (LRP-ICD), which can translocate to the nucleus and interact with Tip60 (27, 28).

Given that BACE and APP interact and traffic with one another, and that APP interacts with and traffics with LRP, we now examined whether LRP interacts with BACE. Using both a FRET-based assay of protein proximity and co-immunoprecipitation, we demonstrate that the LRP-ICD interacts with BACE and that this interaction seems to take place in lipid rafts on the cell surface. Surprisingly, the BACE-LRP interaction does not appear to enhance BACE endocytosis from the cell surface. Instead BACE induces LRP extracellular domain cleavage and subsequent release of the LRP intracellular domain from the membrane. Taken together, these data suggest a close interaction between BACE and LRP on the cell surface

* This work was supported by National Institutes of Health Grants AG12406, AG15379, and P50AG05134, DFG (Deutsche Forschungsgemeinschaft) Grants AR 379/1-1 (to C. A. F. v. A.) and HL50784, HL54710 (to D. K. S.), National Institutes of Health Grant EB00768 (to B. J. B.), the American Federation for Aging Research Beeson-Award, and the J. D. French Alzheimer Foundation (to M. C. I). The costs of publication of this article were defrayed in part by the payment of page charges. This article must therefore be hereby marked "*advertisement*" in accordance with 18 U.S.C. Section 1734 solely to indicate this fact.

§ Both authors contributed equally to this work.

** To whom correspondence should be addressed: Dept. of Neurology/Alzheimer Unit, 114 16th St. (2009), Charlestown, MA 02129. Tel.: 617-726-2299; Fax: 617-724-1480; E-mail: bhyman@partners.org.

[1] The abbreviations used are: BACE, β site of APP-cleaving enzyme; Aβ, amyloid-β; APP, amyloid precursor protein; EEA1, early endosome antigen 1; FLIM, fluorescence lifetime imaging; FRET, fluorescence resonance energy transfer; LC, LRP light chain; LRP, low density lipoprotein receptor-related protein; mLRP, mini-LRP; Ab, antibody; GFP, green fluorescent protein; PBS, phosphate-buffered saline; FITC, fluorescein isothiocyanate; SEAP, secretory alkaline phosphatase; CM, caveolae mambrane; NCM, noncaveolae membrane; DMEM, Dulbecco's modified Eagle's medium; ER, endoplasmic reticulum; siRNA, short interfering RNA; ICD, intracellular domain; CTF, C-terminal fragment; LDL, low density lipoprotein.

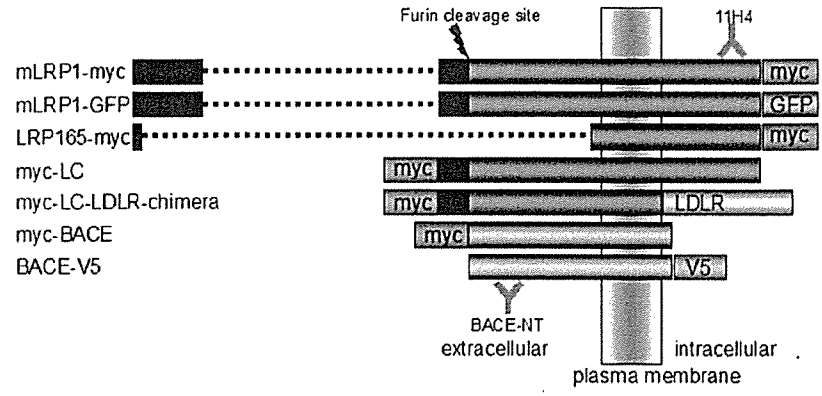

FIG. 1. **Constructs and antibodies used in this study.**

and suggest that LRP is processed by BACE in a fashion analogous to APP processing.

MATERIALS AND METHODS

Generation of Expression Constructs of LRP and BACE and BACE siRNA—The generation of the LRP light chain with two copies of Myc at its N terminus (amino acids 3844–4525) (Myc-LC), the minireceptor mLRP1-Myc that encodes the N-terminal cluster of ligand binding repeats fused to the light chain of LRP and tagged with Myc at its C terminus has been described previously (29). These constructs were used instead of full-length LRP because of its functional similarity to and better expression than full-length LRP. To make mLRP1-GFP, mLRP1 was PCRed into pEGFP-N1 (Clontech). To create the LC-LDLR chimera, a unique KpnI restriction site was introduced into the cytoplasmic portion of LC downstream of the transmembrane domain using the QuikChange XL site-directed mutagenesis kit (Stratagene, La Jolla, CA). PCR-generated sequences encoding cytoplasmic domains of the human LDL receptor were then inserted in place of the LRP sequence. To make the LRP165-Myc construct, mLRP1-Myc was digested, and the band containing the vector and the N-terminal 14 amino acids and the C-terminal 165 amino acids of LRP was extracted and self-ligated as described (27). LRP light chain (amino acid 4148–4544) was fused C-terminally to the Gal4-VP16 synthetic transcription factor, and subcloned into pcDNA3 expression vector (Invitrogen). The leader peptide from LRP was fused to a hemagglutinin epitope, which was then fused to the N terminus of the fusion protein in the construct. Secretory alkaline phosphatase (SEAP) was fused by PCR to the N terminus of LC (amino acids 4018–4525) in pSecTagB (Invitrogen); the SEAP-cDNA was kindly provided by S. F. Lichtenthaler (A. Butenandt-Institut, Munich, Germany).

The Fe65-Myc clone and BACE with N-terminal Myc and C-terminal V5 tags have been described previously (10, 22) as have the phosphorylation site (15) and dileucine mutants of BACE (S498D, S498A, L499A/L500A), BACE-GFP, and the catalytically inactive BACE construct (D93A/D289A) (30). pcDNA3.1-mDab1 was a generous gift from Dr. J. Herz (University of Texas, Dallas, TX). Authenticity of the PCR-generated constructs was confirmed by sequencing. The constructs used in this study are summarized in Fig. 1.

An siRNA corresponding to the *BACE1* gene was designed as described in Kao *et al.* (31) and synthesized by Dharmacon (Lafayette, CO). The following sense sequence was used: 5′-gctttgtggagatggtgga-3′.

Cell Culture Conditions and Transient Transfection—H4 cells derived from human neuroglioma cells, mouse neuroblastoma N2a, pac1, LRP-deficient CHO cells (13-5-1), and HEK293 cells are used in this study. Transient transfection of the cells was performed using a liposome-mediated method (FuGENE 6; Roche Applied Science) according to the manufacturer's instruction. Cells were passaged 24 h prior to transfection and harvested or stained 24 h post-transfection. Primary cortical neurons were prepared as described previously (32). Cortical neurons were isolated from embryonic day 16 CD1 mice (Charles River). Staining was performed 8 days after preparation. For experiments requiring delivery of siRNA, cells were transfected by electroporation per the manufacturer's instructions (AMAXA, Gaithersburg, MD). Specific knockdown of >70% of overexpressing BACE was observed starting 24 h after transfection by Western blot and immunostaining (data not shown).

Immunocytochemistry and Antibodies—Cells were fixed in 4% paraformaldehyde, permeabilized by 0.5% Triton X-100 in TBS, and blocked with 1.5% normal goat serum. For surface staining Triton-X treatment was omitted. The following antibodies were used: the Golgi organelle marker GM130 mAb and the FITC-conjugated endosomal marker EEA1 mAb (BD Transduction Laboratories, San Diego, CA). The tag antibodies used were rabbit anti-Myc Ab (Upstate Biotechnology, Lake Placid, NY), anti-Myc mAb, anti-V5 mAb (both from Invitrogen), and rabbit anti-V5 Ab (Abcam, Cambridge, MA). Antibodies raised in rabbit against the N (46–56) and C termini (487–501) of BACE were obtained from Calbiochem. A hybridoma secreting an mAb to the LRP intracellular domain (11H4) was obtained from the American Type Culture Collection. Alexa-555-labeled cholera toxin B (CTx-B, Molecular Probes, Eugene, OR) was used to visualize lipid rafts. Secondary antibodies used were labeled with FITC and Cy3 (Jackson Immunoresearch, West Grove, PA) or Alexa 488 (Molecular Probes). Immunostained cells were coverslipped and mounted for confocal or two photon microscopic imaging. The immunostained cells were observed with the appropriate filters by confocal microscopy using a Bio-Rad 1024 confocal 3-channel instrument.

Isolation of Caveolae and Noncaveolae Membrane (CM and NCM, respectively)—Caveolae and noncaveolae membrane fractions were isolated from rat smooth muscle cells (pac1) using the method of Smart *et al.* (33). Briefly, 70% confluent rat smooth muscle cells were collected and Dounce-homogenized in a hypertonic buffer containing protease and phosphatase inhibitors. First, the plasma membrane were isolated and sonicated. CM and NCM fractions were prepared using an optiprep gradient with the sonicated plasma membrane samples. 300-μl membrane fractions (PM, CM, NCM) were solubilized with 100 μl of 4× lysis buffer (4% Nonidet P-40, 200 mM Tris, and 600 mM NaCl) to attain final concentration of 1× (1% Nonidet P-40, 50 mM Tris, and 150 mM NaCl). Following the addition of protease and phosphatase inhibitors, CM and NCM lysates were precleared and immunoprecipitated with anti-LRP monoclonal IgG (5A6)-protein G complex overnight. CM and NCM immunoprecipitates along with PM lysate were separated on 4–12% SDS-PAGE under nonreducing conditions and transferred onto nitrocellulose membrane. The membranes were probed with ^{125}I-labeled 11H4 and exposed to Biomax MR film (Kodak).

Cholesterol Depletion—For cholesterol depletion, H4 cells were grown for 24 h in Opti-MEM with 10% fetal bovine serum and then for 24 h in either DMEM supplemented with 2 mM L-glutamine, 10% delipidated fetal bovine serum (Cocalico Biologicals), 20 μM lovastatin (Calbiochem), and 0.5 mM mevalonate (mevalonolactone, Sigma) or DMEM with 10% complete fetal bovine serum (34). Prior to experimentation, cells were incubated for 10 min in DMEM with 10 mM methyl β-cyclodextrin (Mβ-CD, Sigma) or DMEM alone.

Tissue Staining—The Massachusetts Alzheimer Disease Research Center Brain Bank provided temporal cortex. Tissue staining was performed with 11H4 labeled by Alexa-488 and BACE-CT (Calbiochem) labeled by Cy3.

Co-immunoprecipitation—Immunoprecipitation experiments were carried out with BioMag beads conjugated to goat anti-mouse IgG (PerSeptive Biosystems, Framingham, MA). The magnetic beads were incubated overnight at 4 °C with anti-V5 or anti-Myc mAb or TBS alone. Lysates from H4 cells co-transfected with BACE-V5 and mLRP1-Myc or pure lysis buffer were added to the bead-antibody complex for 2 h at 4 °C. After the supernatants were collected, the beads were washed in lysis buffer and then boiled with 2× Tris-glycine SDS sample buffer (Invitrogen) for 3 min. The supernatants were loaded onto 10–20% Tris-glycine polyacrylamide gels (Novex, San Diego, CA) under denaturing and reducing conditions. The proteins were transferred to polyvinylidene difluoride membrane (Millipore, Bedford, MA) and